ELECTRON-BEAM-SHADOWGRAPH FOR THE STUDY OF THE STRONG TURBULENT PLASMA

Ritoku Ando, Naoki Okamoto, Sayaka Shinojima, Satoshi Wada, Hisashi Fujii, Tomohiro Kondo, Norio Toyosugi, and Keiichi Kamada

Faculty of Science, Kanazawa University, 920-1192, Japan

PACS: 52.70.-m

INTRODUCTION

The electron-beam probing technique has an advantage that it does not disturb strongly the field inside the plasma. Electron-beam probing technique normally employs a beam with a small cross-section [1]. The deflection angle of the electron beam is proportional to the line integrated electric field strength. To obtain spatial distribution of the field, the probing beam has to be scanned. However, when the field changes very fast in time and space, the scanning technique can not be available. Therefore, we propose a probing beam with a large cross-section to observe a large area with one-shot. The new technique is practiced using pulse technology. The diagnosis is applied to the unmagnetized plasma, which is perturbed by an intense relativistic electron beam (IREB) for understanding one of the interesting phenomena in plasma physics, *i.e.*, Langmuir turbulence and formation of the collapsing wave packets, "caviton"s.

A number of experiments have been carried out to confirm the strong Langmuir turbulent theory in several fields [2]. The ionospheric-modification experiment with high power radio-frequency wave is one of the fields which have provided a rich proving ground for the theory. The statistical properties of the multi-caviton have been examined. On the other hand, the beam–plasma experiment has many advantages. In the experiments with a low current electron beam, many evidences of the presence of the caviton have been found, for example, the formation of the density well, self-focusing and wave collapsing. But because the energy density is low, the caviton is probably solitary [3]. On the contrary, the experiment with IREB has a possibility to create many cavitons, because the IREB has high energy density. We call it a multiple-caviton system in this paper.

Actually extremely strong electric field is observed spectroscopically inside the plasma after IREB is terminated [4]. The electric field E has the probability distribution, *i.e.*, $\exp(-E^2/ E_m^2)$. The mean field strength E_m is several tens kV/cm. The volume averaged ratio $\langle W \rangle$ of the Langmuir wave energy density, $\varepsilon_0 \langle E^2 \rangle / 4$, to the thermal energy of the plasma electron, $n_p k T_e$, is $\langle W \rangle = \varepsilon_0 \langle E^2 \rangle / 4 n_p k T_e \sim 0.1$, where ε_0 is the free space permittivity, k is the Boltzman constant, n_p is the plasma density, and T_e is the electron temperature.

We have been investigating the IREB-plasma interaction. Our data show that the plasma has many properties found in the study of the Langmuir turbulence. The energy and angular distributions of IREB after the interaction show an existence of large electric field in the plasma. Strong heating of the plasma electron is observed after an IREB injection. Microwave with broadband frequency spectrum is emitted [5]. These data indicate the strong Langmuir turbulence.

Although the IREB-plasma system is a hopeful candidate for the study of the turbulence, there are restraints on the diagnoses, because the IREB emits large noise and the detectors are sometimes damaged. Further more, high-speed response is required on the diagnoses, because the IREB pulse is very short, typically 10 ns to 100 ns. The new technique, named "electron-beam shadowgraph", has advantage to the noise and high response in time.

This paper reports the first data of the new diagnosis. Interesting data are obtained from the IREB-plasma experiment. The experimental data and the strong Langmuir turbulence theory show many good agreements. The shadowgraph technique has the possibility to give the

individual figure of the cavitons, and it might be a powerful diagnosis for investigation of one caviton, and the interaction of multiple cavitons.

EXPERIMENTAL SETUP

The experimental setup is shown in Fig.1 which is similar to the previous experiment where the probing beam with small cross section was employed [6]. A drift chamber, 60 cm long and 16 cm in diameter, is employed.

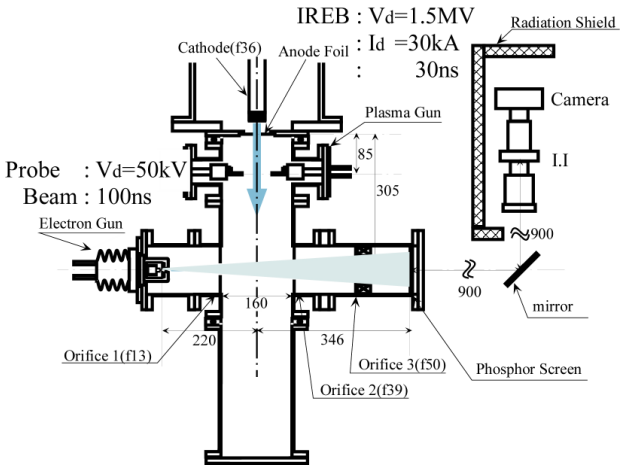

Fig. 1. Experimental setup for the Langmuir turbulence.

No external magnetic field is applied. The plasma is produced by the rail-type guns with carbon rods and the after-glow plasma is utilized. The plasma guns are set at the position of z= 10.0 cm, where z is the distance from the anode. The main component of the plasma is probably carbon, but it contains other components, *e.g.*, hydrogen and oxygen as the impurities. The plasma density, n_p, is measured with a microwave interferometer and Langmuir probes. The n_p at z = 17.5 cm reaches 3 x 10^{13} cm^{-3} at τ =12 μs from the start of the discharge. After the plasma reaches at the chamber wall at τ=20 μs, the n_p is distributed with a gentle slope in the chamber and decrease exponentially in time.

An IREB with energy of 1.5 MeV, current of 30 kA, and duration of 30 ns is injected into the plasma. A thin titanium foil with the thickness of 20 μm is utilized for the anode. About one third of the current can be transported into the drift chamber through the anode. The IREB current is reduced by using a masking plate with many holes by placing after the anode foil.

An electron gun for the probing was set at z= 30.5 cm. The probing beam propagates perpendicularly to the axis of the main chamber. An electron-beam has the energy of 50 kV and the current of ~ 30 mA. A triode type electron gun is used for the probing beam source. A tungsten filament with u-shape is used for the cathode. The distances between the anode, the grid and the cathode are adjusted that the probing beam is defocused and the cross-section increases with the distance from the gun. The distance from the electron gun to the axis of the main chamber is 22.0 cm, and that from the axis to the phosphor screen is 34.6 cm. The projection magnifies the object of the center 2.6 times at the screen. The orifices are set along the path of the probing beam as shown in Fig.1 to reduce the IREB influx to the screen and the electron gun. The diameter of the probing beam is about 7 cm, which is limited by an aperture on the anode of the electron gun. The diameter of the phosphor screen is 10 cm which is larger than the beam diameter. The probing beams with the two different pulse lengths, 100 ns and 1 μs, are employed. The short and long pulses are for taking single photograph and sequential photographs per single discharge respectively.

The luminescence of the phosphor screen is viewed by the camera. In this experiment, the phosphor P47 (AST Ltd., the decay time ~ 25 ns), which has high speed response, is used. The cameras with nanosecond time resolution are introduced. The light noise, *e.g.*, the light which is emitted by hitting of the IREB, is reduced by the nanosecond time response. The light noise which is emitted from the tungsten filament of the electron gun is also reduced, so that the coating on the screen is not necessarily. Because the signal to noise ratio was improved, the lower current density beam with the large cross-section can be utilized.

Two types of high-speed cameras are introduced. One is a conventional high-speed camera for the shingle-shot. An image-intensifier unit (Hamamatsu Photonics, C2925-01) with a microchannel plate is employed for the fast shattering and amplification. A digital camera (Kodak, MDS120) is used for the image capturing, which is remote-controllable with a RS-232 fiber optic modem. Another is the framing camera (IMACON 790, Hadland photonics Ltd.) for the sequential shots.

The exposure time is determined by the pulse length

of the probing beam or the camera. The exposure time of 100 ns is much longer than the Langmuir oscillation period but shorter than the timescale that the ion sound wave propagates. The probing beam can be deflected by both static and oscillating electric fields.

The plasma density n_p is changed by the injection time of the IREB from a start of the discharge, τ. The n_p decreases exponentially as the τ increases. The n_p at τ= 50 μs, 60 μs, 80 μs, 100 μs are n_p= 4 x10^{11} cm^{-3}, 1 x10^{11} cm^{-3}, 4 x10^{10} cm^{-3} and 2 x10^{10} cm^{-3} respectively. The IREB and plasma density ratio, n_b/n_p, becomes about 1 at τ= 80 μs, and 0.01 at τ= 30 μs without the masking plate.

We classify the plasma density n_p into three groups; high (τ < 50 μs), medium (50 μs < τ < 120 μs), and low (120 μs < τ). The observation of the beam pattern can be carried out from the medium n_p to the low n_p. The detail investigation of the shadowgraph was carried out at the medium n_p region. In the high n_p region, the bulk of probing beam receives large shift. Sometimes the beam pattern shifts and the original circle beam is distorted into an ellipse beam. It is often observed that the probing beam is shaved off by the orifice and cannot reach the screen. The detail of the pattern is not well investigated in the high n_p region. In the low n_p region, the observation is possible. The pattern is large compare to the screen size. Because the investigation is difficult, we do not concern it in this paper.

EXPERIMENTAL RESULTS

The examples of the beam pattern are shown in Fig.2. The beam patterns were taken with the 100 ns probing beam and the single shot camera. The dark part on the picture is the location where the electrons hit the screen. In the pictures the large dark circle is the cross-section of the beam. Fig.2 (a) shows the beam pattern without deflection in the case of a vacuum. The original beam pattern is not perfectly homogeneous. Change of the beam

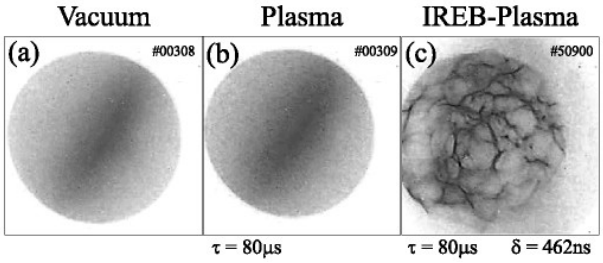

Fig. 2. The beam pattern without and with the deflection; (a) is the original without deflection. (b) is with the plasma. (c) is just after the IREB injection.

pattern will be discussed. The pattern is not affected by the presence of undisturbed plasma, as shown in Fig.2 (b). But the pattern is changed strongly by the participation of the IREB injection.

The typical shadowgraph image after the IREB pulse is characterized by many holes with various sizes, which is called as aggregate holes. Those are observed in Fig.2 (c). From another point of view, the pattern behind the holes consist an irregular mesh. The mesh size, *b*, strongly depends on the plasma density, as shown in Fig.3. The *b* is a few-millimeter at τ= 50 μs, and it becomes several centimeters at τ= 100 μs. The typical scale *b* is shown in each photograph. For example, *b* = 0.36 cm, 0.62 cm, 1.2 cm, 1.9 cm on the screen for τ= 50 μs, 60 μs, 80 μs, 100 μ s, respectively. The *b* is roughly in inverse proportion to the square root of n_p.

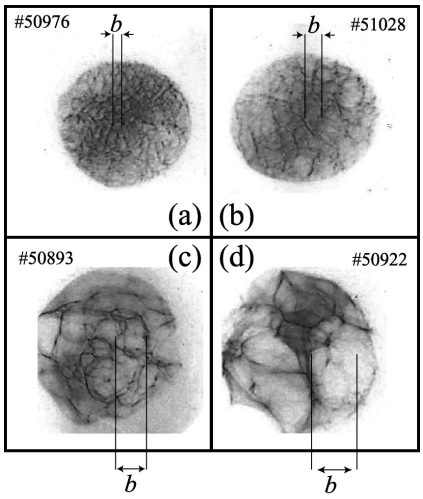

Fig. 3. The mesh size, b, strongly depends on the plasma density. (a) τ= 50 μs, (b) 60 μs, (c) 80 μs, (d) 100 μs. The plasma densities are given in the text. δ= 454 ~488 ns.

The parameter δ is taken as the time interval from the beginning of IREB pulse to the injection of the probing beam. The δ is changed to take the time dependence of the deflection. Following dependencies are observed. (1) At the first 400 ns, clear image can not be observed. The

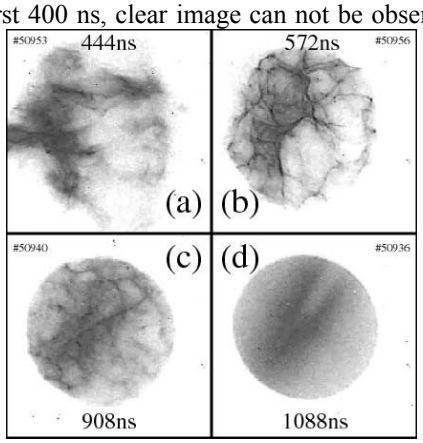

Fig. 4. Typical progress of the pattern after an IREB pulse finished. τ=60 μs.

b is large. (2) Holes are gradually appear and clearly recognized at the time, δ= 450 – 700 ns. (3) At the later time, δ= 700 – 1600 ns, the picture of the holes becomes thinner. The *b* is smaller than the initial. (4) The small circular holes defuse gradually and become thin. It is impossible to observe any deflection after δ > 1600 ns. The typical *b* is changed from 2.5 cm to 1.0 cm when δ is transits from 400 ns to 800 ns at τ= 100 μs.

The time dependence in the single discharge is also observed by the framing camera. 8 photographs of 100 ns/frame with 20 ns exposure are taken in a shot. The positions of the holes are fixed or slowly move in the time interval, although numbers of the holes are overlapped. The size of the hole has a tendency to decrease with time also.

The IREB current is reduced by using the masking plate. The dependence on the IREB density is shown in Fig.5. The IREB current is reduced from 100 % to 4 %. Then the density ratio, n_b/n_p, changes from 0.29 to 0.023. The aggregate holes gradually disappear with the reduction of the IREB current. A number of holes always cover the whole surface of the shadowgraph at the every current. The mesh size, *b*, on the screen decreases due to the reduction of the IREB current. The *b* is changed from 1.25 cm to 0.63 cm at the condition of τ= 100 μs, and from 2.35 cm to 0.90 cm at the condition τ= 80 μs, at the timing of δ= 700 ns. The mesh disappears at the lowest current. The threshold current for the hole becomes higher, if the plasma density is high. It has a stronger correlation with the density ratio n_b/n_p rather than the IREB current. The threshold is estimated about n_b/n_p~ 0.1 for τ= 80 μs, 100 μs, and 120 μs.

DISCUSSION

Because the object is magnified by the dispersed probing beam, the real size should be smaller than that on the screen. The image size *b* on the screen is converted to b_0 by dividing the factor 2.6 by assuming the object is placed on the center position of the plasma column.

The b_0 was roughly in inverse proportion to the square root of n_p in the experiment. Debye length, λ_D, has the same dependence to n_p, the b_0 is supposed to have a relation to λ_D. The λ_D can be roughly estimated from T_e, and n_p. The b_0 corresponds to a few-tens times of λ_D. It is similar to the size of the caviton theoretically.

Theoretically the cavitons reincarnate, if the energy is steadily supplied. In this experiment, the cavitons are considered not to be reformed because the energy input is terminated after the IREB injection.

We calculated the deflection due to the caviton by the Runge-Kutta-Gill method. We presume both the strength and the size of the electric field from the strong turbulence theory.

Following assumptions are utilized. (1) The characteristic size of caviton is a, the field strength at the center is E_0, and the energy density ratio is $W = \varepsilon_0 E_0^2 / 4 n_p k T_e$. (2) The Gaussian profile is employed for the envelope of the oscillating field. (3) The energy density of the electric field at the caviton center is equal to the thermal energy density of the plasma when the a is minimum. (4) The "self-similarity condition" is taken into consideration. The condition implies that the product of the size and the field strength is kept constant at the collapse. (5) For the simplicity, we approximate that the field oscillates with the plasma frequency of the back ground plasma. (6) After the burnout, the oscillating field disappears and the density dip is remained. The bipolar electrostatic field, which is produced from the density inequality between thermal electrons and the ion density well, is taken into account by $kT_e \ln(n_p)/e$.

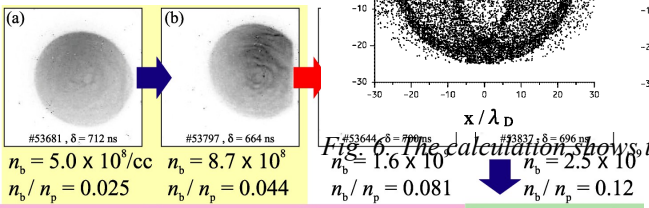

Fig. 5. The beam density is decreased with keeping plasma density constant, τ=100 μs.

A solid beam with the circular cross section is interacted with a caviton. The example of the shadowgraph of the single caviton is shown in Fig.6. The scale on the axis is normalized by λ_D. Figure 6 (a) is the pattern due to the oscillating field. The potential which gives the oscillating field has two poles at $x = \pm a/\sqrt{2}$. The poles attract and repulse the beam when the electric field oscillates. A low density hole and a high density peak are produced and superposed at the location of the each pole. A deeper hole with elliptic shape is produced at the center of the caviton by the overlap of these holes. On the contrary the high density part makes the sharp walls at the periphery. The hole observed in the experiment can be explained by the deflection due to the caviton. Because the sharp walls are produced at the peripheries, the pattern is also explained. The corrected mesh size b_0 is nearly

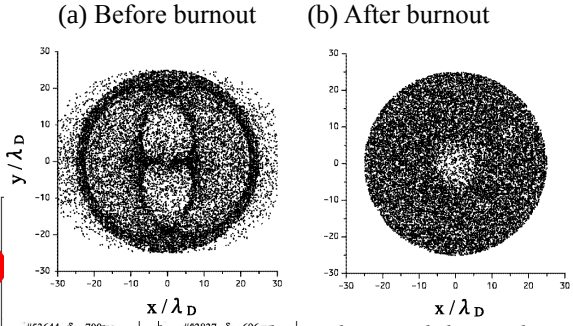

Fig. 6. The calculation shows the possibility to detect the caviton image in this experimental condition. W= 1.0, a= 10 λ_D, L=36.5 cm, and the linear polarization are assumed.

equal to $\sqrt{2}a$. The change of b with the reduction of the IREB current can be attributed to T_e.

The beam electrons which pass through near the center of the caviton are deflected strongly. Those come outside of the bulk of the beam on the screen, as seen in the fig. 6 (a). The maximum deflection angle, θ_{max}, can be calculated by the simple equation: $\theta_{max} = \theta_0 \exp(-\xi^2)$, and $\xi = a' \sqrt{kT_e / 8eV_0}$, where eV_0 is the energy of the probing beam, and $a' = a/\lambda_D$. θ_0 is the theoretical deflection angle when the phase of the oscillating field does not change, which is given by $\theta_0 = \sqrt{\pi} \cdot aE(0)/2V_0 = \sqrt{\pi\Theta} \cdot kT_e / eV_0$. Θ is the constant of the collapse, and it is defined in ref. [2]. The maximum angle is estimated as $\theta_{max} \sim$ 0.018rad, when V_0= 50 kV, kT_e/e = 50 eV, and Θ= 100. Although the θ_{max} is small, the shift is observable on the screen. By assuming the distance, L, between the caviton and the screen as L =36.5 cm, the shift can be calculated, $L\,\theta_{max}$ = 0.66 cm. The amplitude of the shift is $2L\,\theta_{max}$= 1.3 cm. The broadening of the point beam was about 1 cm in the previous experiment. It is similar to the evaluated value.

Following situation can be considered. Multiple

cavitons are formed in the duration of the IREB pulse. The caviton size is large and the image is not clear just after the IREB injection, because ξ is large. The caviton undergoes collapse and narrows the size, a, in the next moment. The projected image becomes clear with the time progress. Many holes and walls can be recognized. Characteristic size of those holes decreases as the caviton collapses. If the a becomes enough small, *e.g.* $10\lambda_D$, the oscillating field dissipates and the density hole is remained, *i.e.*, burnouts. It makes the electrostatic field and the small circular holes in the shadowgraph. Fig. 6 (b) is the pattern due to the electrostatic field which is remained after the oscillating field dissipates. The deflection makes a small circular hole. The pattern is smaller than the one before the burnout. As the density well relaxes, the image is considered to be disappeared.

The proper circumstance for applying the shadowgraph technique is following. First, the caviton must have a proper size for the measurement. Second, the deflection must provide proper angle or proper contrast for the observation. The contrast is the function of the ratio, $L\,\theta_{max}/a$, of the maximum shift, $L\,\theta_{max}$, to the caviton size a. If the ratio takes the value near 1, the contrast is visible. Because the condition is satisfied in the experiment, it is reasonable that the hole can be observed.

Because we do not know exact T_e, we cannot discuss the situation precisely. The measurement of the plasma parameters is important to confirm the conclusion of the turbulence. Conclusively the IREB-plasma experiment has a possibility to provide the rich ground for the study of multiple caviton system by the introduction of the new diagnosis.

ACKNOWLEDGEMENTS

We appreciate to Prof. Ivan N. Onishchenko, for his supports. He encouraged us from the early stage of the study. A part of this work is supported by a Grant-in-Aid for Scientific Research from Ministry of Education, Science, Sports and Culture, Japan.

REFERENCES

1. R. S. Harp, *et al.*, *Rev. Sci. Instrum.* 36, 960-968 (1965)
2. P. A. Robinson, *Rev. Modern Phys.*, **69**, 507-573 (1997).
3. A. Y. Wong, and P. Y. Cheung, *Phys. Rev. Lett.*, **52**, 1222 (1984).
4. G. Benford and X.-L. Zhai, *Phys. Fluids* B, **5**, 1914-1916 (1993)
5. R. Ando, *et al.*, *J. Phys. Soc. Jpn.*, **65**, 2518-2521 (1996).
6. R. Ando, et al.., *IEEE trans. Plasma Sci.*, **27**, 1545-1547 (1999).